



CHORUS

This is the accepted manuscript made available via CHORUS. The article has been published as:

Intraband conductivity response in graphene observed using ultrafast infrared-pump visible-probe spectroscopy

K. M. Dani, J. Lee, R. Sharma, A. D. Mohite, C. M. Galande, P. M. Ajayan, A. M. Dattelbaum, H. Htoon, A. J. Taylor, and R. P. Prasankumar

Phys. Rev. B **86**, 125403 — Published 4 September 2012

DOI: [10.1103/PhysRevB.86.125403](https://doi.org/10.1103/PhysRevB.86.125403)

Intraband conductivity response in graphene observed using ultrafast infrared-pump, visible-probe spectroscopy

K. M. Dani^{1,2*}, J. Lee^{1*}, R. Sharma^{3,4}, A. D. Mohite¹, C. M. Galande⁵, P. M. Ajayan⁵, A. M. Dattelbaum¹, H. Htoon¹, A. J. Taylor¹, and R. P. Prasankumar^{1#}

¹*Center for Integrated Nanotechnologies, Los Alamos National Laboratory, Los Alamos, NM
87545*

²*Okinawa Institute of Science and Technology, Okinawa, Japan, 904-0495*

³*Theoretical Division, Los Alamos National Laboratory, Los Alamos, NM 87545*

⁴*TRIUMF, 4004 Wesbrook Mall, Vancouver, BC, V6T 2A3, Canada*

⁵*Department of Mechanical Engineering and Materials Science, Rice University, Houston, TX
77005*

**These authors contributed equally to this work.*

#Email: rpprasan@lanl.gov

ABSTRACT:

Graphene, a truly two-dimensional (2D) material with a unique linear energy-momentum dispersion, demonstrates novel photonic properties like universal absorption & conductivity with applications including terahertz (THz) lasing, broadband mid-infrared (IR) detectors and tunable ultrafast lasers. Understanding the ultrafast non-equilibrium dynamics of photocarriers in graphene's unique relativistic band structure is important for the development of such high-speed, graphene-based photonic devices as well as from a fundamental point of view. Here, our experiments indicate the relativistic nature of a non-equilibrium gas of electrons and holes

photogenerated in a graphene monolayer as early as 100 femtoseconds (fs) after photoexcitation. We observe a nonlinear scaling in the Drude-like optical conductivity of the photocarriers with respect to their density, in striking contrast to the linear scaling expected from conventional materials with parabolic dispersion relations. Our measurements also indicate that hot photocarriers cool on a sub-100 fs timescale via interactions with optical phonons. These results elucidate the unique nature of the ultrafast dynamics of photocarriers in a relativistic material, in contrast to conventional materials, and provide a way to manipulate graphene's optical conductivity for applications in photonics and plasmonics.

I. INTRODUCTION

Graphene, a monoatomic layer of carbon atoms arranged in a hexagonal pattern, presents a unique opportunity, from a materials science perspective, to pursue novel fundamental physics and applications, as charge carriers are governed by the relativistic Dirac equation instead of the Schrodinger equation used for conventional materials. The resulting zero-gap, linear energy-momentum dispersion relationship in graphene has led to novel demonstrations like the anomalous quantum Hall effects^{1,2}, Klein paradox³ and universal conductivity and absorption^{4,5}. From an applied perspective, graphene exhibits useful optoelectronic properties with applications in photovoltaics and touch-screens^{6,7}. In particular, the universal conductivity of graphene (i.e., the constant, frequency-independent value of its optical conductivity)^{4,5} has enabled photonic applications over a wide range of the electromagnetic spectrum, from low energy THz devices⁸ to ultrafast mid-IR detectors⁹ to tunable ultrafast lasers in the near-IR^{10,11}. Such demonstrations are leading to numerous other ideas in graphene-based photonic devices and applications⁶. However, to fully utilize graphene's potential in photonic devices and applications, particularly for high-speed photonics, it is necessary to understand the non-equilibrium behavior of the electron-hole plasma generated by femtosecond photoexcitation in the context of its relativistic band structure. Just as the above-mentioned equilibrium studies in graphene have revealed interesting physics, one reasonably expects intriguing non-equilibrium dynamics as well in this relativistic material, as recent results have begun to demonstrate^{12,13,14}.

Previous studies on the ultrafast non-equilibrium dynamics of graphene have demonstrated carrier-carrier interactions on the order of tens of femtoseconds^{15,16,17,18,19}, ultrafast carrier-

phonon scattering^{19,20} and electron-hole recombination on the order of a few picoseconds (ps)^{21,22}. However, a demonstration of the relativistic nature of a non-equilibrium photoexcited gas of electrons and holes, distinguishing it from plasmas in conventional materials with parabolic band structures, has remained elusive.

In this Letter, we indicate the relativistic nature of a non-equilibrium electron-hole plasma in graphene as early as 100 fs after photoexcitation. In a counterintuitive visible pump-probe experiment (Figure 1a), we isolate the Drude-like contribution to the optical conductivity of the photoexcited electron-hole plasma. Therein, we find that our data is best fit by a \sqrt{N} dependence on the electron-hole plasma density N , in striking contrast to the expected linear dependence on N observed for non-relativistic charge carriers in conventional materials with parabolic band dispersions^{23,24}. We also observe the $\frac{1}{\omega^2}$ frequency dependence, where ω is the frequency, expected from the Drude response of plasmas in general – both relativistic and non-relativistic. To the best of our knowledge, these are the first experiments that indicate the relativistic nature of a photoexcited electron-hole plasma in graphene on an ultrafast timescale. In addition, our results reveal a rapid cooling of the electron-hole plasma within 100 fs via interaction with optical phonons. These techniques also suggest ways to isolate and control the different contributions to the optical conductivity in graphene for applications in photonic devices and plasmonics.

II. EXPERIMENTAL DETAILS

The sample studied here was grown via chemical vapor deposition (CVD) on a Cu substrate, using hexane as a liquid precursor²⁵. The graphene was then transferred from the Cu substrate onto an MgO substrate. The Raman spectrum shown in Figure 1b reveals that our graphene film predominantly consists of a monolayer (since the ratio of the 2D and G peaks is ~ 2)²⁶. In addition, our sample is unintentionally hole-doped with a chemical potential $\mu_h \sim 130$ meV ($\sim 1.2 \times 10^{12}$ holes/cm²)²⁷. Ultrafast visible pump-probe experiments were performed using an 800 nm, 250 kHz regeneratively amplified Ti:sapphire laser system. A portion of the laser output was used as a pump pulse to photoexcite carriers in a ~ 220 μm diameter spot on the sample. The remaining laser output was directed to an optical parametric amplifier to generate visible probe pulses tunable from 1.74-2.42 eV (512-713 nm), leading to a system temporal resolution of ~ 100 fs. By delaying the probe pulse with respect to the pump pulse, we measured the time-resolved photoinduced reflectivity changes in the sample at different probe photon energies (ω_{probe}) and for different photoexcitation densities (pump fluence ~ 0.2 -1 mJ/cm²). The graphene interband absorption is given by $2Z_0\sigma_Q/(n_s+1)^{15}$, where $\sigma_Q = e^2/4\hbar$ is the frequency-independent interband conductivity of graphene^{4,5}, Z_0 is the vacuum impedance, and $n_s=1.72$ is the refractive index of the MgO substrate. We thus calculate that 1.7% of the incident pump pulse is absorbed, which is then used to calculate N . We have measured the linear absorption of our sample to be constant, and consistent with this value over the range of photoexcitation intensities used here. All measurements were performed at room temperature.

III. RESULTS

Figure 2(a) shows the time-resolved photoinduced reflectivity change, $\Delta R/R$, for several values of N at $\omega_{probe} = 1.77 eV$. We also show $\Delta R/R$ (1.55 eV), taken at a carrier density of $N = 1.36 \times 10^{12} cm^{-2}$ in a degenerate pump-probe experiment using the same laser system, in Figure 2(b) for comparison with the corresponding 1.77 eV trace and with previous work^{16-19,22}. This shows that the peak amplitude of $\Delta R/R$ at 1.55 eV is over a factor of three higher than at 1.77 eV, as expected, but the signal-to-noise ratio in our experiments is more than sufficient to obtain high quality data at all probe photon energies. For all N , we see a two-component relaxation in the $\Delta R/R$ signal, with a fast relaxation on a timescale of a few hundred fs and a slower relaxation component of ~ 1.4 ps (inset of Fig. 2(b)), as previously observed by other groups^{15,21,22}. In this paper, we will explore the relativistic nature of the photoexcited electron-hole plasma by focusing on the peak $\Delta R/R$ signal that occurs within the 100 fs temporal resolution of our pump-probe measurement, which is measured as a function of N and ω_{probe} .

In Figure 3, we plot the peak $\Delta R/R$ signal versus N at fixed $\omega_{probe} = 1.77 eV$ (Figure 3a (circles)) and versus ω_{probe} at fixed $N = 3.1 \times 10^{13} cm^{-2}$ (Figure 3b (circles)). In conventional materials with parabolic band dispersion, the component of the $\Delta R/R$ signal due to the Drude response of photoexcited carriers would scale linearly with N . However, in Fig. 3a, we note the striking nonlinearity in the data. In particular, Fig. 3c, depicting data taken on the same sample in a separate measurement that focuses on low photoexcitation densities, shows that a \sqrt{N} fit best describes the data rather than a linear fit, confirming the trend shown in Fig. 3a. We observe this trend at all measured probe frequencies. This does not rule out the possibility that more complex functions (e.g., non-power-law functions) could fit our data; however, we focus on the \sqrt{N}

dependence since it can be clearly linked to the intrinsic physical properties of graphene, as shown by the detailed analysis and modeling described in the next section. To the best of our knowledge, this has not been observed in previous work, perhaps due to the different photoexcitation density ranges and pump/probe frequencies used in those studies¹⁵⁻²². In the following discussion, we explain this nonlinear behavior in graphene, which originates from its unique linear dispersion, unlike the nonlinear processes often observed in semiconductors²⁸.

IV. MODELING AND DISCUSSION

To understand the photoinduced response of graphene, we explicitly analyze the real parts of the two contributions to graphene's optical conductivity – the *interband* contribution, σ_{inter} , due to electronic transitions between the valence band and the conduction band, and the *intraband* contribution, σ_{intra} , resulting from electron (hole) transitions within the conduction (valence) band. For ideal, undoped graphene at zero temperature, $\sigma_{intra}=0$, while the interband conductivity σ_{inter} is given by σ_Q ^{4,5}. For finite temperatures T and non-zero intrinsic doping levels (denoted by a hole Fermi energy of μ_h for our p-doped sample), general expressions for the real parts of σ_{inter} and σ_{intra} have been derived²⁹. These result in an interband contribution that is given by a step function with an onset at $2\mu_h$, a step height of σ_Q and a step-width of $k_B T$ (Figure 4a). The intraband contribution shows a Drude-like $\frac{\gamma}{\omega^2 + \gamma^2}$ dependence on the frequency (Figure 4b), where γ is the scattering rate.

Upon photoexcitation with the 1.5 eV pump pulse, we assume that the carriers quickly thermalize amongst themselves and with the intrinsic holes on a tens of femtoseconds timescale^{15,19} that is not resolved within our ~ 100 fs temporal resolution. We also assume a partial loss of energy to optical phonon modes on this 100 fs timescale due to fast electron-phonon scattering, as supported by previous work^{12,19,20}. We note that several recent studies have indicated that intensity-dependent processes such as Auger recombination and impact ionization could cause the photoexcited state to collapse into a single thermalized Fermi-Dirac distribution on a sub-100 fs time scale, instead of maintaining separate electron and hole Fermi energies^{12,18,30}. To address this issue in the context of our experiments, we have performed time-resolved photoemission experiments on samples grown and measured under similar conditions as ours. The results clearly reveal separate electron and hole Fermi energies for the first few hundred fs, which evolve into a single thermalized Fermi-Dirac distribution within a few ps³¹. These results are consistent with the picture that interband recombination due to carrier-carrier interactions is suppressed in graphene's linear band structure, thereby separately conserving the photoexcited electrons and holes with separate Fermi levels^{6,11,32}. Thus we describe the new photoexcited state by modified hole and electron Fermi energies $\tilde{\mu}_h, \tilde{\mu}_e$, respectively, and an increased temperature \tilde{T} to account for the excess energy remaining in the photoexcited carriers (Figure 1a).

The photoexcited state changes both components of the conductivity as follows: a) The step-like interband conductivity shifts to $2\tilde{\mu}_h$; it develops a negative conductivity step below $2\tilde{\mu}_e$ due to the possibility of stimulated electron-hole recombination^{8,33} and the step widths are now given by $k_B\tilde{T}$ (Figure 4a). b) The intraband conductivity increases at all frequencies due to the

additional carriers (Figure 4b). Thus, at *high* enough probe photon frequencies, the *change* in conductivity due to photoexcitation is dominated by σ_{intra} . The *change* in σ_{inter} is negligible for frequencies above $(2\tilde{\mu}_h + k_B\tilde{T})/\hbar$. We note that in contrast to most semiconductors, the possibility of interband stimulated emission in graphene^{8,33} prevents one from isolating the intraband dynamics of carriers at terahertz frequencies, as is normally done³⁴. Instead, we use this counterintuitive visible pump-probe technique to isolate the Drude-like, intraband response. More generally, this illustrates ways to separately control and manipulate the σ_{intra} and σ_{inter} contributions to graphene's optical conductivity using pump-probe spectroscopy (i.e., by tuning the pump and probe photon energies). Each contribution has its own importance in graphene-based applications (e.g., σ_{intra} mimics the physics of far-away relativistic particles as in neutron stars and white dwarfs, σ_{inter} results in the properties of universal absorption and conductivity) and their novel interplay has also led to recent proposals in graphene-based plasmonics³⁵ and photonics.

The general expressions for the real parts of the inter- and intra-band conductivities in the presence of an unequal number of holes and electrons at finite temperatures are given by^{15, 29}:

$$\begin{aligned}\sigma_{inter} &= \sigma_Q \frac{1}{2} \left[\tanh\left(\frac{\hbar\omega - 2\tilde{\mu}_h}{4k_B\tilde{T}}\right) + \tanh\left(\frac{\hbar\omega - 2\tilde{\mu}_e}{4k_B\tilde{T}}\right) \right] \\ \sigma_{intra} &= \sigma_Q \frac{4k_B\tilde{T}}{\pi\hbar} \left[\ln\left(1 + e^{\frac{\tilde{\mu}_h}{k_B\tilde{T}}}\right) + \ln\left(1 + e^{\frac{\tilde{\mu}_e}{k_B\tilde{T}}}\right) \right] \frac{\gamma}{\omega^2 + \gamma^2}\end{aligned}\quad (1)$$

For a given photoexcitation density N , the values of $\tilde{\mu}_h, \tilde{\mu}_e, \tilde{T}$ are determined by number and energy conservation: $\tilde{N}_h = N_h + N$; $\tilde{N}_e = N$; $U_h + \Delta Q = \tilde{U}_h + \tilde{U}_e + \tilde{U}_{phonons}$, where $N_h(\tilde{N}_h)$ are

the number of holes before (after) photoexcitation; \tilde{N}_e is the number of electrons after excitation; U_h is the energy in the intrinsic hole gas before excitation; ΔQ is the energy absorbed from the pump pulse; and $\tilde{U}_h, \tilde{U}_e, \tilde{U}_{phonons}$ are the energies in the holes, electrons and phonons, respectively, after photoexcitation. Given a $\sim 25\sim 50$ fs carrier-optical phonon scattering time for carriers of energy $\hbar\omega/2 = 0.75\text{eV}$, we assume about three optical phonon emissions (at 175 meV) per photoexcited carrier within the 100 fs pulse width^{19,20}. These assumptions are supported by recent theoretical²⁰ and experimental^{12,19} work on energy exchange between photoexcited carriers and optical phonons in graphene. The number and energy of electrons and holes are given by the first and second order Fermi integrals¹⁵, respectively. The values for chemical potential and temperature $\tilde{\mu}_h, \tilde{\mu}_e, \tilde{T}$ are numerically obtained to satisfy these conservation equations; these calculations and assumptions are described in more detail in the Appendix. For the highest photoexcitation densities under consideration, this gives $\tilde{T} \approx 600\text{K}$. We also note that without assuming such a partial loss of energy to phonon modes, the resulting ~ 4000 K electron-hole gas would exhibit decreased conductivity upon photoexcitation, which corresponds to a negative photoinduced change in reflectivity. This is not consistent with our data, where the photoinduced change in reflectivity is positive. Thus, our data supports a rapid (sub-100 fs) and significant loss of energy from photoexcited quasiparticles to optical phonons.

For the remainder of our analysis, we approximate $\tilde{T} = 600\text{K}$ for all carrier densities (see Appendix), $\tilde{\mu}_h = \hbar v \sqrt{\tilde{N}_h \pi}$ and $\tilde{\mu}_e = \hbar v \sqrt{\tilde{N}_e \pi}$, where $v = 10^6 \text{ m/s}$ is the Fermi velocity in graphene. For the highest carrier densities ($N = 3.68 \times 10^{13} \text{ cm}^{-2}$) we get $\tilde{\mu}_h = 0.72 \text{ eV}$ and $\tilde{\mu}_e = 0.70 \text{ eV}$. Figure 3a shows the change in conductivity (total, interband and intraband) versus N at a

fixed probe frequency of $\omega_{probe} = 1.77 eV$. As discussed above, the interband conductivity contributes minimally to the total change for lower carrier densities, while the dominant Drude-like intraband conductivity scales as \sqrt{N} (Fig. 3c). This is understood by noting that for $k_B \tilde{T} \ll \tilde{\mu}_h, \tilde{\mu}_e$, one can approximate $\ln\left(1 + e^{\tilde{\mu}/k_B T}\right) \approx \frac{\tilde{\mu}}{k_B \tilde{T}}$ (Eq. (1)). Thus, $\Delta\sigma_{intra} \propto \mu_h + \mu_e \propto \sqrt{N}$ for $N \gg N_h$, which is the case for all values of N examined here. The fact that $\frac{\Delta\sigma}{\sigma} \propto \frac{\Delta R}{R}^4$ and a \sqrt{N} function gives the best fit to our data for $\frac{\Delta R}{R}$ as compared to a linear function (Fig. 3c) indicates that the electron-hole plasma behaves relativistically at femtosecond timescales. For the largest N , $2\tilde{\mu}_h \rightarrow \hbar\omega_{probe}$ and we see that σ_{inter} also begins to contribute to the photoinduced reflectivity change. We note that the observation of the \sqrt{N} scaling in $\frac{\Delta\sigma}{\sigma} \propto \frac{\Delta R}{R}^4$ implies that \mathcal{Y} is constant over the range of photoexcitation densities under consideration. This situation could arise as a result of the interplay between various scattering mechanisms, including carrier-carrier, carrier-photon, and carrier-impurity scattering³⁶.

Figure 3b shows the photoinduced change in conductivity versus ω_{probe} at a fixed photoexcitation density. As before, the Drude-like intraband conductivity dominates for $\hbar\omega_{probe} > 2\tilde{\mu}_h$. The experiment (circles) closely follows the $\frac{\gamma}{\omega^2 + \gamma^2}$ behavior expected from the Drude-like model of intraband conductivity (Eq. (1)). At lower probe energies, $\hbar\omega_{probe} \approx 2\tilde{\mu}_h$ and the interband conductivity plays an important role in the photoinduced reflectivity change.

V. CONCLUSION

Our experiments indicate the relativistic nature of a non-equilibrium electron-hole plasma in monolayer graphene within 100 fs of photoexcitation. With a counterintuitive visible pump-probe experiment, we isolated the Drude-like intraband optical conductivity of the electron-hole plasma and observed that it scales as \sqrt{N} , in stark contrast to the linear Drude response of charge carriers in conventional materials with parabolic energy-momentum dispersion. Furthermore, our measurements indicate a rapid loss of energy from the photoexcited carriers to optical phonon modes within 100 fs. These results contribute to the development of high-speed photonic applications in a unique, relativistic material, and the experimental technique used here provides a way to separately control and manipulate the different contributions to graphene's optical conductivity, which has applications in fundamental relativistic physics, photonics and plasmonics.

References:

-
- ¹ Y. Zhang, Y.-W. Tan, H. L. Stormer, and P. Kim, *Nature* **438**, 201-204 (2005).
- ² K. I. Bolotin, F. Ghahari, M. D. Shulman, H. L. Stormer, and P. Kim, *Nature* **462**, 196-199 (2009).
- ³ M. I. Katsnelson, K. S. Novosely, and A. K. Geim, *Nature Phys.* **2**, 620-625 (2006).
- ⁴ K. F. Mak, M. Y. Sfeir, Y. Wu, C. H. Lui, J. A. Misewich, and T. F. Heinz, *Phys. Rev. Lett.* **101**, 196405 (2008).
- ⁵ R. R. Nair, P. Blake, A. N. Grigorenko, K. S. Novoselov, T. J. Booth, T. Stauber, N. M. R. Peres, and A. K. Geim, *Science* **320**, 1308 (2008).
- ⁶ F. Bonaccorso, Z. Sun, T. Hasan, and A. C. Ferrari, *Nature Photonics* **4**, 611 (2010).
- ⁷ S. Bae, H. Kim, Y. Lee, X. Xu, J.-S. Park, Y. Zheong, J. Balakrishnan, T. Lei, H. R. Kim, Y. I. Song, Y.-J. Kim, K. S. Kim, B. Özyilmaz, J.-H. Ahn, B. H. Hong, and S. Iijima, *Nature Nano.* **4**, 574-578 (2010).
- ⁸ M. Ryzhii, A. Satou, T. Otsuji, A. A. Dubinov, and V. Y. Aleshkin, *J. Appl. Phys.* **106**, 084507 (2009).
- ⁹ F. Xia, T. Mueller, Y.-M. Lin, A. Valdes-Garcia, and P. Avouris, *Nature Nano.* **4**, 839 (2009).
- ¹⁰ W. D. Tan, D. Tang, X. Xu, J. Zhang, C. Xu, F. Xu, L. Zheng, L. Su, and J. Xu, *Opt. Exp.* **18**, 16739-16744 (2010).
- ¹¹ Z. Sun, D. Popa, T. Hasan, F. Torrisi, F. Wang, E. J. R. Kelleher, J. C. Travers, and A. C. Ferrari, *ACS Nano* **4**, 803 (2010).
- ¹² C. H. Lui, K. F. Mak, J. Shan, and T. F. Heinz, *Phys. Rev. Lett.* **105**, 127404 (2010).
- ¹³ W.-T. Liu, S. W. Wu, P. J. Schuck, M. Salmeron, Y. R. Shen, and F. Wang, *Phys. Rev. B* **82**, 081408(R) (2010).

-
- ¹⁴ R. J. Stóhr, R. Kolesov, J. Pflaum, and J. Wrachtrup, Phys. Rev. B **82**, 121408(R) (2010).
- ¹⁵ H. Choi, F. Borondics, D. A. Siegel, S. Y. Zhou, M. C. Martin, A. Lanzara, and R. A. Kaindl, Appl. Phys. Lett. **94**, 172102 (2009).
- ¹⁶ P. Plochocka, P. Kossacki, A. Golnik, T. Kazimierczuk, C. Berger, W. A. de Heer, and M. Potemski, Phys. Rev. B **80**, 245415 (2009).
- ¹⁷ F. Carbone, G. Aubock, A. Cannizzo, F. Van Mourik, R. R. Nair, A. K. Geim, K. S. Novoselov, and M. Chergui, Chem. Phys. Lett. **504**, 37 (2011).
- ¹⁸ D. Sun, Z.-K. Wu, C. Divin, X. Li, C. Berger, W. A. de Heer, P. N. First, and T. Norris, Phys. Rev. Lett. **101**, 157402 (2008).
- ¹⁹ H. Wang, J. H. Strait, P. A. George, S. Shivaraman, V. B. Shields, M. Chandrashekhar, J. Hwang, F. Rana, M. G. Spencer, C. S. Ruiz-Vargas, and J. Park, Appl. Phys. Lett. **96**, 081917 (2010).
- ²⁰ F. Rana, P. A. George, J. H. Strait, J. Dawlaty, S. Shivaraman, M. Chandrashekhar, and M. G. Spencer, Phys. Rev. B. **79**, 115447 (2009).
- ²¹ P. A. George, J. Strait, J. Dawlaty, S. Shivaraman, M. Chandrashekhar, F. Rana, and M. G. Spencer, Nano Lett. **8**, 4248-4251 (2008).
- ²² J. M. Dawlaty, S. Shivaraman, M. Chandrashekhar, F. Rana, and M. G. Spencer, Appl. Phys. Lett. **92**, 042116 (2008).
- ²³ W. J. Padilla, “*Light-Matter Interactions,*” in *Optical Techniques for Solid-State Materials Characterization*, edited by R. P. Prasankumar and A. J. Taylor (CRC Press, Boca Raton 2011).
- ²⁴ M. Dressel and G. Gruner, *Electrodynamics of Solids* (Cambridge University Press, Cambridge 2002).

-
- ²⁵ A. Srivastava, C. Galande, L. Ci, L. Song, C. Rai, D. Jariwala, K. F. Kelly, and P. M. Ajayan, *Chem. Mater.* **22**, 3457-3461 (2010).
- ²⁶ A. C. Ferrari, J. C. Meyer, V. Scardaci, C. Casiraghi, M. Lazzeri, F. Mauri, S. Piscanec, D. Jiang, K. S. Novoselov, S. Roth, and A. K. Geim, *Phys. Rev. Lett.* **97**, 187401 (2006).
- ²⁷ A. Kasry, M. A. Kuroda, G. J. Martyna, G. S. Tulevski, and A. A. Bol, *ACS Nano* **4**, 3839-3844 (2010).
- ²⁸ K. Sokolowski-Tinten and D. von der Linde, *Phys. Rev. B* **61**, 2643 (2000).
- ²⁹ L. A. Falkovsky and A. A. Varlamov, *Eur. Phys. J. B.* **56**, 281-284 (2007).
- ³⁰ T. Winzer, A. Knorr, and E. Malic, *Nano Letters* **10**, 4839 (2010)
- ³¹ S. Gilbertson, G. L. Dakovski, T. Durakiewicz, J.-X. Zhu, K. M. Dani, A. D. Mohite, A. Dattelbaum, and G. Rodriguez, *J. Phys. Chem. Lett.* **3**, 64 (2012).
- ³² J. González, F. Guinea, and M. A. H. Vozmediano, *Phys. Rev. Lett.* **77**, 3589 (1996).
- ³³ T. Li, L. Luo, M. Hupalo, J. Zhang, M. C. Tringides, J. Schmalian, and J. Wang, *Phys. Rev. Lett.* **108**, 167401 (2012).
- ³⁴ R. A. Kaindl, R. Huber, B. A. Schmid, M. A. Carnahan, D. Hägele, and D. S. Chemla, *Phys. Stat. Sol. (b)* **243**, 2414 (2006).
- ³⁵ A. Vakil and N. Engheta, *Science* **332**, 1291 (2011).
- ³⁶ S. D. Sarma, S. Adam, E. H. Hwang, and E. Rossi, *Rev. Mod. Phys.* **83**, 402 (2011).

Acknowledgments:

This work was performed at the Center for Integrated Nanotechnologies, a U.S. Department of Energy, Office of Basic Energy Sciences user facility and also partially supported by the NNSA's

Laboratory Directed Research and Development Program. Los Alamos National Laboratory, an affirmative action equal opportunity employer, is operated by Los Alamos National Security, LLC, for the National Nuclear Security Administration of the U. S. Department of Energy under contract DE-AC52-06NA25396. We gratefully acknowledge financial support and stimulating interactions with colleagues through the University of California Office of the President's (UCOP) program on Carbon Nanostructures.

Figure Legends:

Figure 1. (Color online) Schematic depicting photo-doping of graphene through femtosecond optical excitation and the room temperature Raman spectrum of single layer graphene. (a) Electron and hole Fermi energies before (μ_h) and after ($\tilde{\mu}_h, \tilde{\mu}_e$) ultrashort pulsed photoexcitation, with $\mu_h \sim 130$ meV due to unintentionally doped holes. (b) Raman spectrum showing the G peak at 1580 cm^{-1} (196 meV), D peak around 1350 cm^{-1} (167 meV), and 2D peak around 2700 cm^{-1} (335 meV). The intensity ratio of 1:2 between the G and 2D peaks confirms that our sample predominantly consists of a graphene monolayer.

Figure 2. (Color online) (a) Transient photo-induced reflectivity changes at different photoexcited carrier densities, with $\omega_{probe} = 1.77$ eV. (b) Transient photo-induced reflectivity

change at $\omega_{probe}=1.55, 1.77$ eV for $N=1.36 \times 10^{12}$ cm $^{-2}$. The inset shows curve fits to the $\omega_{probe}=1.77$ eV data.

Figure 3. (Color online) Peak change in $\Delta R/R$ as a function of the photoexcited carrier density, N , and probe photon energy, ω_{probe} . (a) Peak change in $\Delta R/R$ as a function of N for $\omega_{probe}=1.77$ eV. The intraband conductivity dominates the signal for all but the highest carrier densities, and the data thus follows the \sqrt{N} dependence (solid blue line) exhibited by relativistic two-dimensional Dirac quasiparticles. (b) Peak change in $\Delta R/R$ as a function of ω_{probe} for $N=3.1 \times 10^{13}$ cm $^{-2}$. The intraband contribution (solid blue line) dominates when $\omega_{probe} > 2\tilde{\mu}_h$, following a simple Drude-like response that is proportional to $\propto 1/\omega^2$. The decrease in signal amplitude at low photon energies comes from the interband component (solid green line). (c) Peak change in $\Delta R/R$ as a function of N for $\omega_{probe}=1.77$ eV in the region where the intraband conductivity dominates the signal ($N < 3 \times 10^{13}$ cm $^{-2}$). Power law (black) and linear (red) fits demonstrate that a \sqrt{N} function fits our data rather than a linear function.

Figure 4. (Color online) Schematic depicting the conductivity changes induced by photoexcited carriers. In the purple (left) shaded region, both interband and intraband components contribute to the total conductivity change, while in the yellow (right) shaded region only the intraband component contributes. Therefore, at high probe photon energies ($\omega_{probe} > 2\tilde{\mu}_h$), the photoinduced change in total conductivity is dominated by the intraband conductivity change, with effectively no contribution from changes in the interband conductivity.

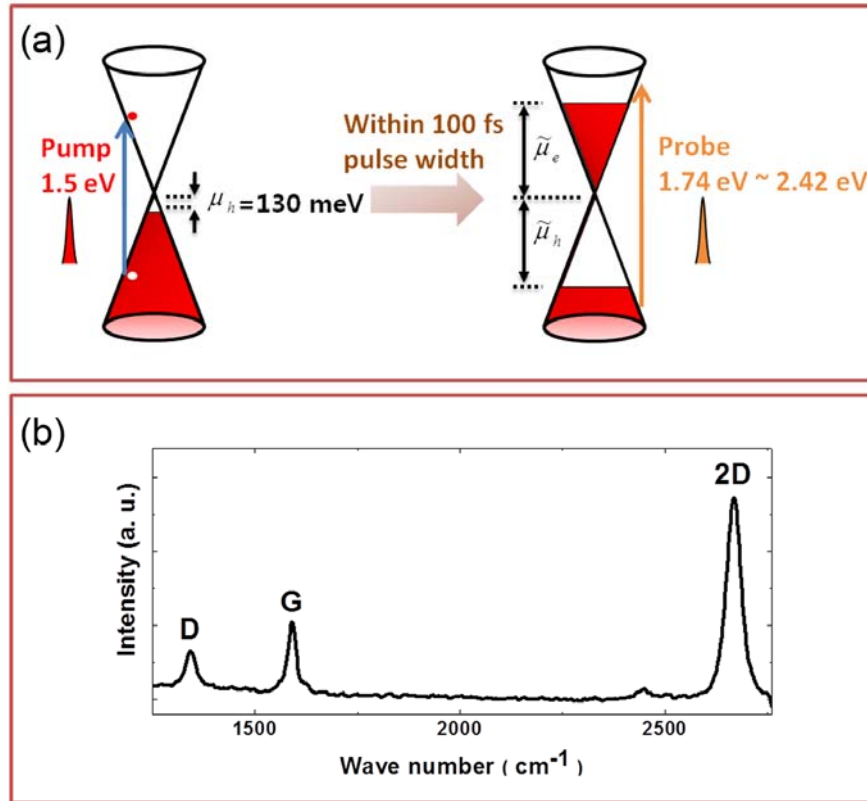


Figure 1. (Color online) Schematic depicting photo-doping of graphene through femtosecond optical excitation and the room temperature Raman spectrum of single layer graphene. (a) Electron and hole Fermi energies before (μ_h) and after ($\tilde{\mu}_h, \tilde{\mu}_e$) ultrashort pulsed photoexcitation, with $\mu_h \sim 130$ meV due to unintentionally doped holes. (b) Raman spectrum showing the G peak at 1580 cm^{-1} (196 meV), D peak around 1350 cm^{-1} (167 meV), and 2D peak around 2700 cm^{-1} (335 meV). The intensity ratio of 1:2 between the G and 2D peaks confirms that our sample predominantly consists of a graphene monolayer.

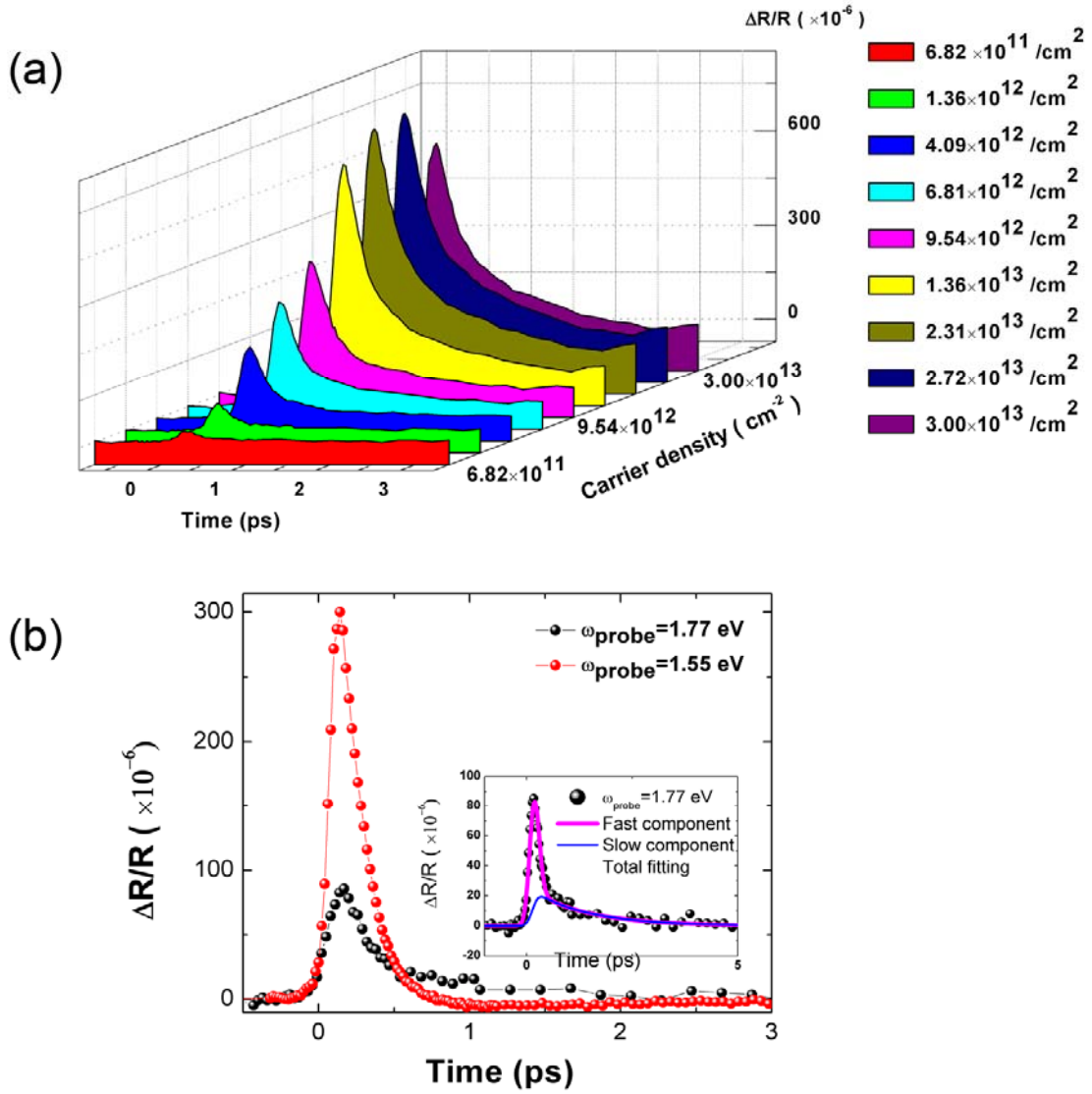


Figure 2. (Color online) (a) Transient photo-induced reflectivity changes at different photoexcited carrier densities, with $\omega_{\text{probe}} = 1.77 \text{ eV}$. (b) Transient photo-induced reflectivity change at $\omega_{\text{probe}} = 1.55, 1.77 \text{ eV}$ for $N = 1.36 \times 10^{12} \text{ cm}^{-2}$. The inset shows curve fits to the $\omega_{\text{probe}} = 1.77 \text{ eV}$ data.

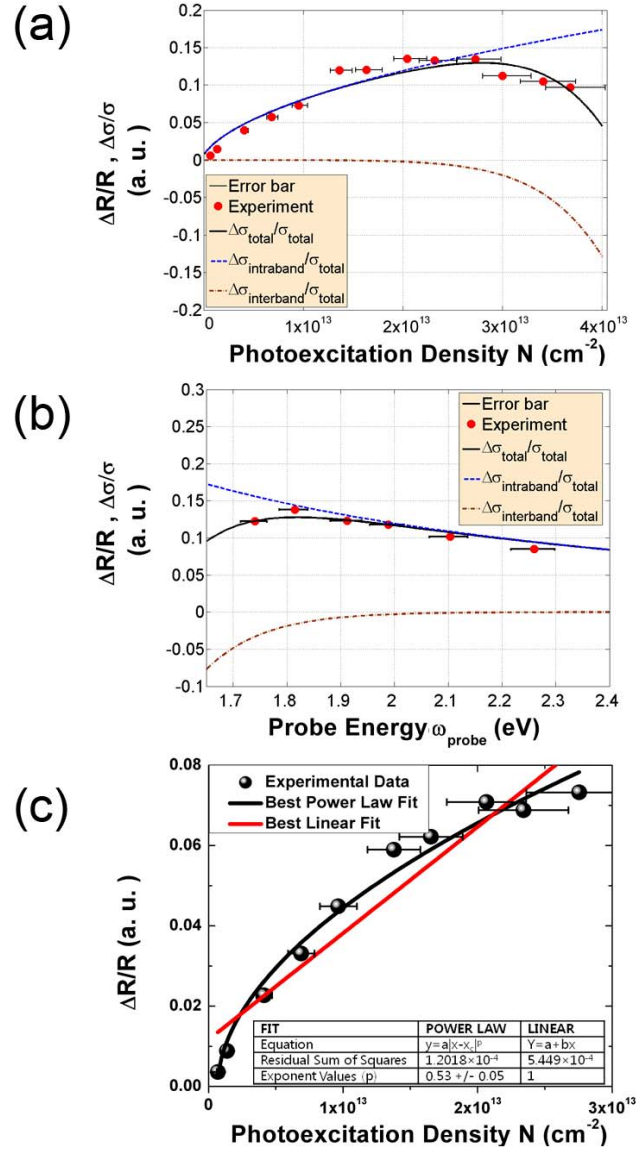


Figure 3. (Color online) Peak change in $\Delta R/R$ as a function of the photoexcited carrier density, N , and probe photon energy, ω_{probe} . (a) Peak change in $\Delta R/R$ as a function of N for $\omega_{probe} = 1.77$ eV. The intraband conductivity dominates the signal for all but the highest carrier densities, and the data thus follows the \sqrt{N} dependence (solid blue line) exhibited by relativistic two-

dimensional Dirac quasiparticles. (b) Peak change in $\Delta R/R$ as a function of ω_{probe} for $N=3.1 \times 10^{13} \text{ cm}^{-2}$. The intraband contribution (solid blue line) dominates when $\omega_{probe} > 2\tilde{\mu}_h$, following a simple Drude-like response that is proportional to $\propto 1/\omega^2$. The decrease in signal amplitude at low photon energies comes from the interband component (solid green line). (c) Peak change in $\Delta R/R$ as a function of N for $\omega_{probe}=1.77 \text{ eV}$ in the region where the intraband conductivity dominates the signal ($N < 3 \times 10^{13} \text{ cm}^{-2}$). Power law (black) and linear (red) fits demonstrate that a \sqrt{N} function fits our data much better than a linear function.

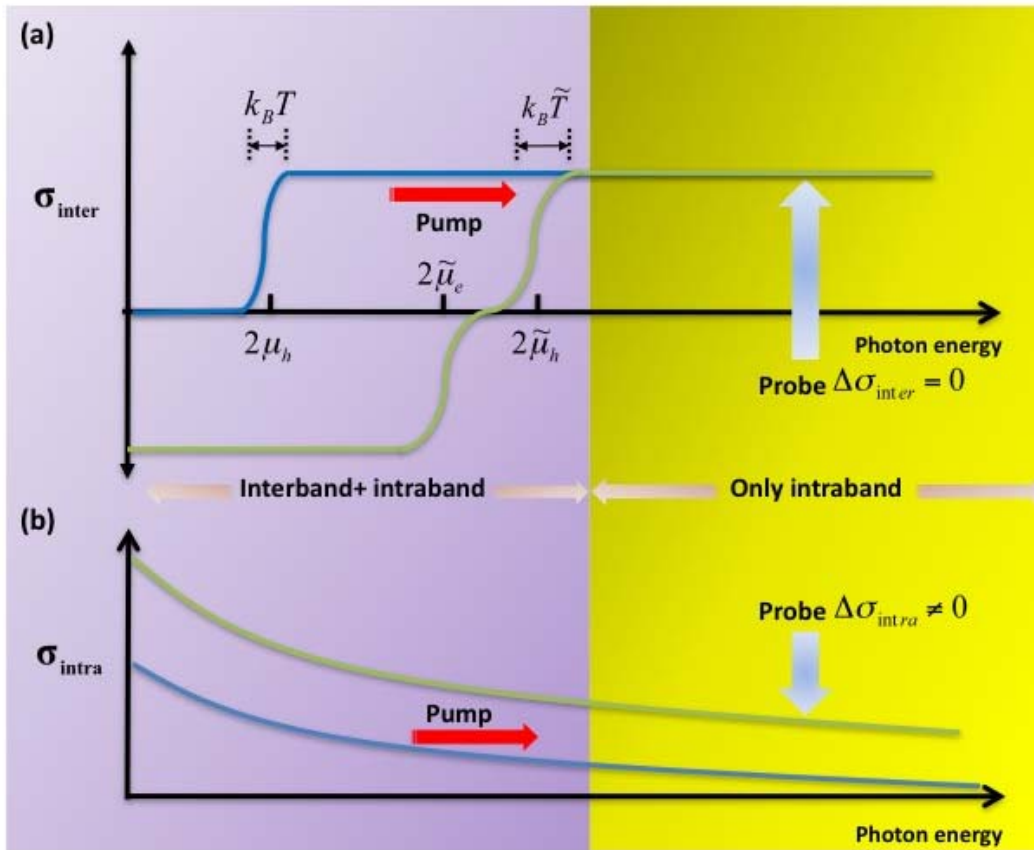


Figure 4. (Color online) Schematic depicting the conductivity changes induced by photoexcited carriers. The blue and green curves depict the (a) interband and (b) intraband contributions to the conductivity before and after photoexcitation, respectively. In the purple (left) shaded region, both interband and intraband components contribute to the total conductivity change, while in the yellow (right) shaded region only the intraband component contributes. Therefore, at high probe photon energies ($\omega_{probe} > 2\tilde{\mu}_h$), the photoinduced change in total conductivity is dominated by the intraband conductivity change, with effectively no contribution from changes in the interband conductivity.

APPENDIX: ANALYSIS OF THE TEMPERATURE OF PHOTOEXCITED CARRIERS

Here, we explore the temperature of the photoexcited carriers on short timescales. Before the graphene sample is photoexcited by the pump pulse, we assume that the electrons, optical phonons, and acoustic phonons are in thermal equilibrium with each other and with the environment. This defines the initial state of the graphene monolayer.

The graphene sample used in our experiments has a small hole doping density of $N_h=1.2\times 10^{12}/\text{cm}^2$, which corresponds to a negative electronic chemical potential $\mu_e = -130$ meV. In the following discussion, it will be convenient to describe the valence band by the electron vacancies, i.e. holes, and the conduction band by electrons. The initial state, therefore, has a hole chemical potential $\mu_h = 130$ meV and an initial electron chemical potential $\mu_e = -130$ meV. The electron and hole gases are in thermal equilibrium with each other and with the environment at $T=300$ K.

Photoexcitation involves shining a pump laser of wavelength 800 nm, corresponding to a photon energy of $\omega_p = 1.55$ eV, on the graphene sample. Electrons absorb the energy from the incident pump pulse. By varying the power of the pulse, we vary the photoexcited carrier density, N . The energy transferred to the electron and hole gases per unit area is given by $\Delta Q=N\times \omega_p$ (where ΔQ is defined after Eq. 1). Assuming that each photon is absorbed by one electron in the valence band, the number density of electrons and holes is $\tilde{N}_e=N$ and $\tilde{N}_h=N_h+N$, respectively.

Let us first try to understand qualitatively how the system will evolve from this initial state. The fastest process is the energy exchange between the multitude of excited electrons and holes in the system.²⁰ This thermalizes the electron and hole gas at a fairly high temperature, as large as 4000 K. The next fastest step is expected to be the exchange of energy between electrons and phonons. This turns out to be very important because this occurs on a timescale of a few hundred fs, comparable to the time resolution of our experiment. At a timescale of a few ps, the electrons and holes recombine with each other. Eventually, the graphene monolayer exchanges energy with the substrate and the environment and relaxes back to the original configuration.

Now let us consider the evolution of the system in greater detail, focusing on the effect of photoexcitation on the carrier density and the temperature, both of which affect the conductivity that we observe. As mentioned above, the fastest time scale is given by the interaction between the electrons and holes, and leads to a rapid thermalization of the electron and hole gases between themselves and amongst each other, on a time scale of about 10 fs. At this point, the number of electrons (holes) is given by \tilde{N}_e (\tilde{N}_h). This is a good assumption because the recombination time scale is over 100 times longer and hence the electron and hole numbers can be taken to be separately conserved. Treating the charge carriers as Fermi gases at a temperature T gives us the relations¹⁵

$$\begin{aligned}\tilde{N}_e &= 4 \int \frac{d^2k}{(2\pi)^2} \frac{1}{e^{(\varepsilon(k) - \tilde{\mu}_e)/T} + 1} \\ \tilde{N}_h &= 4 \int \frac{d^2k}{(2\pi)^2} \frac{1}{e^{(\varepsilon(k) - \tilde{\mu}_h)/T} + 1}\end{aligned}\tag{A1}$$

where $\varepsilon(k) = v|k|$ is the dispersion relation of the charge carriers in graphene, with $v \approx 1/300c$, and c is the speed of light. Also, since the electrons and holes have not yet shared their energy with the other components of the system, energy conservation tells us that

$$U_h + \Delta Q = 4 \left[\int \frac{d^2k}{(2\pi)^2} \frac{\varepsilon(k)}{e^{(\varepsilon(k) - \tilde{\mu}_e)/T} + 1} + \int \frac{d^2k}{(2\pi)^2} \frac{\varepsilon(k)}{e^{(\varepsilon(k) - \tilde{\mu}_h)/T} + 1} \right] \quad (\text{A2})$$

By solving the three equations simultaneously, one can find the chemical potentials $\tilde{\mu}_h$, $\tilde{\mu}_e$ and the temperature T for various photoexcitation densities N . This corresponds to the black curve in Figure A1, where we plot the temperature of the charge carriers as a function of N .

From 10–100 fs, the electrons and holes can exchange energy with the phonons.²⁰ In our system, the state of graphene at $t \sim 100$ fs has special importance, because this is the temporal resolution of our pump-probe experiment. Furthermore, the peak of the measured conductivity is typically located at $t \sim 100$ fs. Since it is this peak value that we compare with the theoretically expected behavior, we now describe the state of the photoexcited graphene at $t \sim 100$ fs in some detail.

The electrons interact with both the optical and the acoustic phonons. For the present calculation, we will include only energy exchange with optical phonons, with the motivation that the emission of a single optical phonon reduces the energy of the electron by ~ 175 meV. The electron-phonon energy exchange is described by the following rate equations,²⁰

$$R_{\Gamma LO} = R_{\Gamma TO} = \frac{9}{4} \left(\frac{dt}{db} \right)^2 \frac{1}{\pi \rho \omega_{\Gamma O} \hbar^4 v^4} \int_0^{\hbar \omega_{\Gamma O}} dE E (\hbar \omega_{\Gamma O} - E) f(E - \tilde{\mu}_e) [1 - f(E - \hbar \omega_{\Gamma O} - \tilde{\mu}_e)] [1 + n_{Op} \hbar \omega_{\Gamma O}] \quad (\text{A3})$$

Here $R_{\Gamma LO}$ and $R_{\Gamma TO}$ represents the zone-center LO and TO phonon scattering rate per cc and

ω_{FO} and n_{OP} are the optical phonon frequency and occupation number, respectively. dt/db is related to the change in electronic energy due to a change in carbon-carbon bond length, and f is the Fermi distribution function for the electrons.²⁰ We can calculate the initial rate by approximating the initial density of optical phonons to be zero. The emission rate of optical phonons by a photoexcited electron (or hole) can be found by dividing the scattering rate per unit volume by the number density of the respective carriers. The mass density of graphene is $\rho = 7.6 \times 10^{-7} \text{ kg/m}^2$. Estimates for the coefficient dt/db range from 45 eV/nm to 70 eV/nm. Using these values we find that a charge carrier emits an optical phonon every 25 – 50 fs.

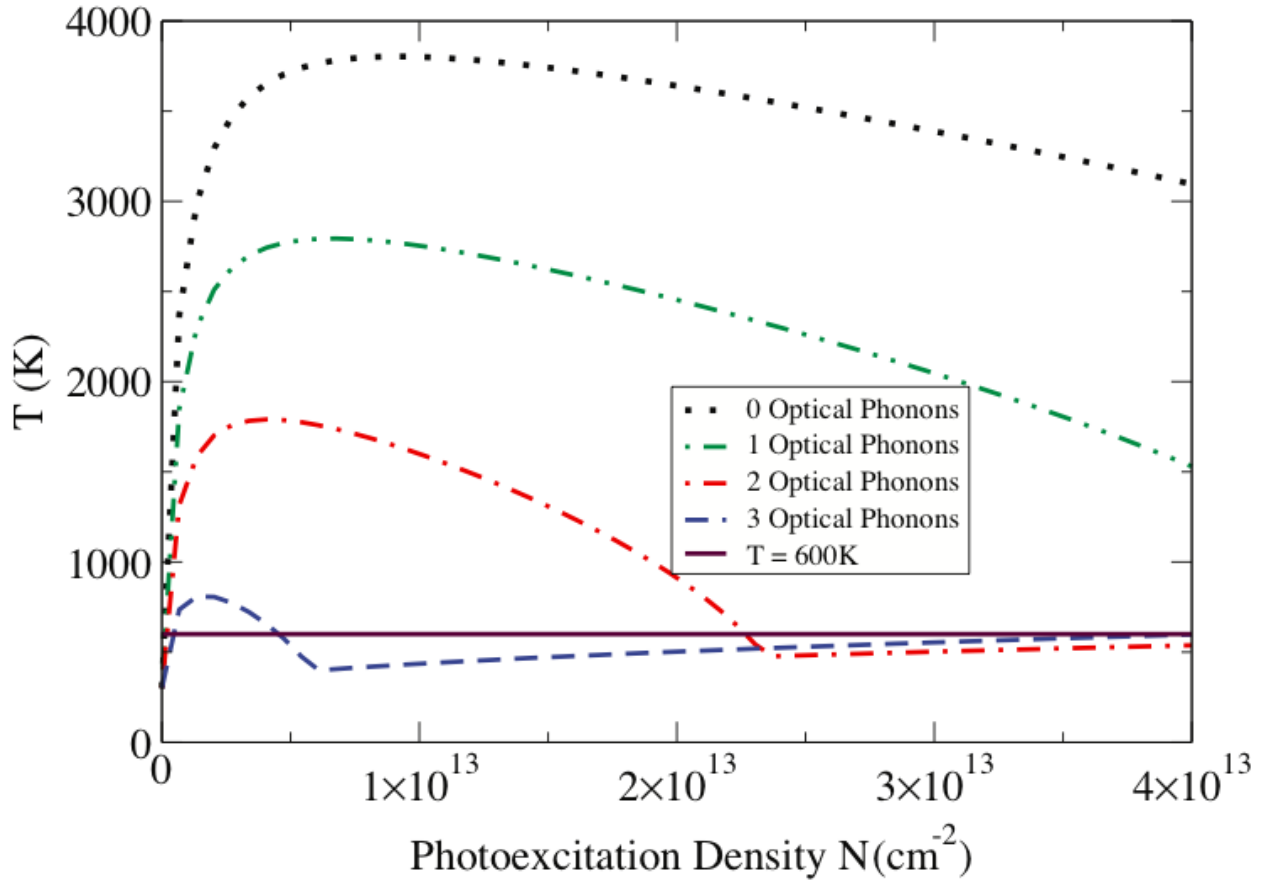


Figure A1. Temperature as a function of photoexcited carrier density, calculated by assuming 0-3 optical phonon emissions per carrier.

Therefore, in 100 fs, we expect an emission of roughly 2 – 4 optical phonons per photoexcited charge carrier. The optical phonons can also redistribute energy among each other, and a rough estimate of their energy distribution can be obtained by assuming that they thermalize at a temperature T_{op} , so that the energy density of the optical phonons is

$$U_{phonon} = 2 \int_{k \in B} \frac{d^2k}{(2\pi)^2} \frac{\varepsilon(k)_{OP}}{e^{\varepsilon(k)_{OP}/T} - 1}, \quad (\text{A4})$$

where $\varepsilon(k)_{OP}$ is the dispersion relation of the optical phonons and the integral of k runs over the modes in the Brillouin zone. Since the dispersion of the optical phonons is reasonably flat, we approximate the integral by taking $\varepsilon(k)_{OP} = \hbar\omega_{\Gamma O}$ to be constant. There are two optical modes [20] of frequencies 160 meV and 190 meV in graphene, so to simplify the equations we approximate them by a single mode with an average frequency $\hbar\omega_K = 175 \text{ meV}$ with a degeneracy factor of 2. Then the integral over k just gives the volume of the Brillouin zone. Finally, the entire Brillouin zone is not excited because of momentum conservation, and we take this into account by multiplying the density of states by a factor $f_B < 1$. In our calculation we take f_B to be 0.05. Our results do not change substantially if we vary f_B within a factor of two.

$$U_{phonon} \sim f_B 2.596 \left(\frac{4\pi}{3\sqrt{3}a} \right)^2 \frac{\hbar\omega_K}{e^{\omega_K/T} - 1} = 19.64 \hbar\omega_K / \text{cm}^2 \quad (\text{A5})$$

$$\tilde{U}_h + \tilde{U}_e = U_h + \Delta Q - U_{phonon} \quad (\text{A6})$$

Now we have all the ingredients to describe our calculation of the temperature of the carrier gas at $t \sim 100$ fs. Assuming that every photocarrier emits (on average) 2 – 4 optical phonons of energy 175 meV, we find that on this time scale, the temperature of the carrier gas is significantly reduced from its initial value (black curve in Fig. A1). We show the temperature

curves calculated by assuming 1, 2 and 3 phonon emissions in Fig. A1. In particular, for three phonon emissions per carrier (blue curve) we obtain a temperature that is comparable to 600 K (yellow line) throughout the carrier density range of interest. This calculation also gives the values of $\tilde{\mu}_e$ and $\tilde{\mu}_h$.

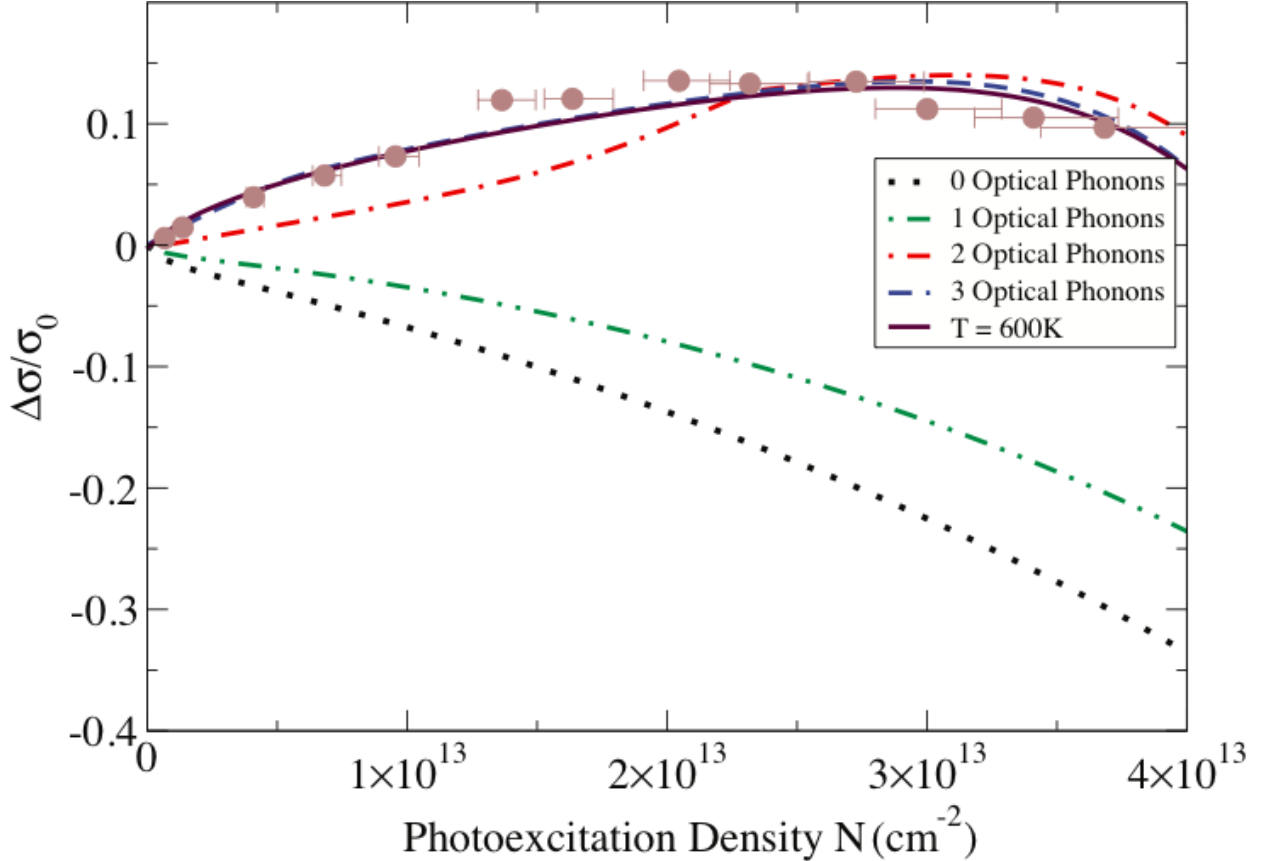


Figure A2. Conductivity as a function of photoexcited carrier density, calculated by assuming 0-3 optical phonon emissions per carrier.

With T , $\tilde{\mu}_e$ and $\tilde{\mu}_h$ in hand, we can calculate the conductivity as a function of the photoexcited carrier density, shown in Figure A2. The colors are the same as in Fig. A1. We see that the result for three phonon emissions is very similar to the result for $T = 600$ K, and also matches well with our experiments (brown circles, identical to those in Fig. 3a of the manuscript), justifying our use of a constant $T = 600$ K in section IV of our paper.